An Enhanced Linear Active Disturbance Rejection Rotor Position Sensorless Control for Permanent Magnet Synchronous Motors

Lizhi Qu , *Student Member, IEEE*, Wei Qiao , *Senior Member, IEEE*, and Liyan Qu, *Senior Member, IEEE*

Abstract—An enhanced linear active disturbance rejection controller (ELADRC) based rotor position sensorless field-oriented control scheme for the permanent magnet synchronous motor (PMSM) drivers is proposed in this article. The ELADRC consists of two linear extended state observers (LESOs) and a proportional current controller. One LESO is designed to estimate the back electromotive force (EMF), which is treated as the external disturbance. Then, the rotor position and speed are obtained from the estimated back EMF without any phase delay or chattering problem. The other LESO is designed to estimate the internal disturbances, such as the parameter and current regulation quality variations. The estimated total disturbance is used as a feedforward compensation term in the current control loop to improve the current regulation quality of the plant, which further improves the rotor position estimation performance. The plant combined with the two LESOs is equivalent to an integrator with a unity gain, which is controlled by a simple proportional current controller to generate the desired voltage vector for the pulsewidth modulation operation. Finally, the stability of the closed-loop PMSM drive system with the ELADRC-based scheme is analyzed. Based on the analysis, the parameters of the ELADRC are designed. The proposed scheme is validated by the experimental results for a 275-W salient-pole PMSM drive in which the PMSM is similar to the traction motor used in Toyota Prius hybrid electric vehicles at a reduced scale.

Index Terms—Field-oriented control (FOC), linear extended state observer (LESO), linear active disturbance rejection control (LADRC), permanent magnet synchronous motor (PMSM), rotor position estimation, sensorless control.

I. INTRODUCTION

PERMANENT magnet synchronous motors (PMSMs) have been widely employed in industrial applications due to their high reliability, high efficiency, and high power density [1], [2]. The field-oriented control (FOC) control systems of PMSM drives commonly use rotor position sensors, such as hall-effect sensors, optical encoders, or resolvers for a closed-loop current

regulation. To reduce the cost and improve the reliability of the PMSM drive systems, rotor position sensorless FOC has been widely researched over the past few decades [3]–[15].

There are two major categories of rotor position sensorless FOC methods for the salient-pole PMSMs. One is based on the back electromotive force (EMF) estimation [3]–[8] and the other is based on the high-frequency (HF) signal injection [9]–[11]. For the standstill and low-speed operations, an HF signal injection-based method is commonly used to observe the rotor position by utilizing the saliency of a salient-pole PMSM since the value of the back EMF is too small to be estimated accurately. For medium- and high-speed operations, a back EMF estimation based method is mainly adopted to obtain the rotor position by observing the back EMF. The HF signal injection-based method is not suitable in this case due to the limited control bandwidth. To achieve a rotor position sensorless FOC for the entire speed operating range, a combination of the two methods is needed.

For some specific applications, e.g., the traction motors of the hybrid electric vehicles, the performance of the observer in medium- and high-speed operations is more important. In such an application, the sliding-mode observer (SMO) is a promising solution. In several previous works [3]–[8], the SMO has been applied to the sensorless PMSM drives due to its simple algorithm and high robustness to the system structure and parameter variations. The defects of the conventional SMO are the chattering and phase delay problems, which have been partially solved by using the improved SMOs with sigmoid functions and a separate back EMF observer [12], [13]. To solve the problems completely, disturbance observers [14], [15] were proposed based on the back EMF model in the stationary reference frame or a rotating reference frame. By selecting proper observer gains, the stability of the disturbance observers can be guaranteed. However, it is usually not easy to design the gains of the disturbance observers due to some factors. First, the variations of the machine parameters used in the observers affect the accuracy of the position estimation, especially when both the d- and q-axis inductances have cross saturations. Moreover, since the measured currents are the inputs of the position observers, the current regulation quality and the position estimation will affect each other in the closed-loop sensorless FOC.

Recently, a new method called the active disturbance rejection control (ADRC) [16], [17] has attracted considerable attention due to its intrinsic ability of disturbance rejection and simple

The authors are with the Power and Energy Systems Laboratory, Department of Electrical and Computer Engineering, University of Nebraska−Lincoln, Lincoln, NE 68588-0511 USA (e-mail: lizhi.qu@huskers.unl.edu; wqiao3@unl.edu; lqu2@unl.edu).

design process without the need for an accurate system model. The ADRC has been applied in motor drives [18], [19]. In [18], a robust control scheme using three first-order ADRCs was presented for the speed control of induction motor drives without the need for a rotor flux estimation, which reduced the computing cost. In [19], a hybrid sensorless FOC scheme combining an ADRC-based HF current injection method with another ADRC-based back EMF method for the rotor position estimations in low- and high-speed regions, respectively, for PMSMs was presented. Although the hybrid scheme is better than the conventional SMO-based sensorless FOC scheme in the steady-state conditions, the rotor position estimation performance may be unsatisfactory in transient conditions, and current regulation quality was not considered in [19]. Moreover, the parameter turning of the ADRCs was complex.

This article proposes a novel enhanced linear ADRC (ELADRC) based rotor position sensorless FOC scheme for PMSM drives in an estimated synchronously rotating reference frame. The ELADRC consists of two linear extended state observers (LESOs) and a proportional current controller. One LESO is designed to estimate the back EMF, which is treated as an external disturbance, without using any low-pass filter or switching function. Then, the rotor position and speed are obtained from the estimated back EMF by using a tracking controller consisting of back EMF normalization and a phase-locked loop (PLL) without any phase delay or chatting problem. The other LESO is designed to estimate the internal disturbances, such as the parameter and current regulation quality variations of the PMSM drive to improve the current regulation, which further increases the rotor position estimation accuracy. The estimated total disturbance is used to compensate the output of the current controller to generate the input to the plant. In this way, the plant combined with the two LESOs is equivalent to an integrator, which can be controlled by a simple proportional current controller to generate the desired voltage vector for the pulsewidth modulation control of the PMSM inverter. The stability of the closed-loop PMSM drive system with the proposed ELADRC-based sensorless FOC scheme is analyzed. Based on the analysis, the parameters of the ELADRC are designed. The effectiveness of the ELADRC-based sensorless FOC scheme is evaluated by a 275-W salient-pole PMSM drive in which the PMSM is similar to the traction motor used in Toyota Prius hybrid electric vehicles at a reduced scale.

II. Proposed Linear Active Disturbance Rejection Control (LADRC) Based Sensorless FOC Scheme Without Considering PMSM Parameter Variations

A. LADRC-Based Rotor Position Estimation Algorithm

A back EMF based model for a salient-pole PMSM can be expressed in the synchronously rotating dq reference frame according to Morimoto *et al.* [15] as follows:

$$\begin{bmatrix} v_{sd} \\ v_{sq} \end{bmatrix} = \begin{bmatrix} R_s + pL_d & -\omega_{re} \cdot L_q \\ \omega_{re} \cdot L_q & R_s + pL_d \end{bmatrix} \begin{bmatrix} i_{sd} \\ i_{sq} \end{bmatrix} + \begin{bmatrix} 0 \\ \eta \end{bmatrix} \quad (1)$$

where v_{sd} and v_{sq} are the d- and q-axis stator voltages, respectively; i_{sd} and i_{sq} are the d- and q-axis stator currents,
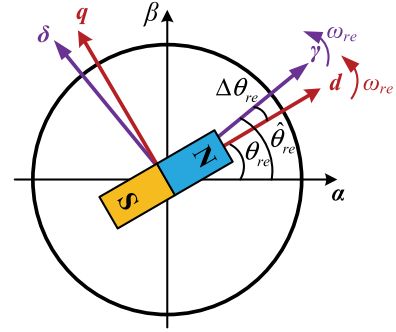

Fig. 1.   Estimated $\gamma\delta$ reference frame and the dq reference frame.

respectively; R_s is the stator armature resistance; L_d and L_q are the d- and q-axis stator inductances, respectively; ω_{re} is the rotor electrical angular speed; $p = d/dt$ is the time derivative operator; and η is the magnitude of the back EMF, which is expressed as

$$\eta = (L_d - L_q) \cdot (\omega_{re} \cdot i_{sd} - pi_{sq}) + \omega_{re} \cdot \psi_m \quad (2)$$

where ψ_m is the rotor magnetic flux linkage.

However, in a sensorless FOC drive system, such a dq model cannot be utilized since the rotor position θ_{re} is not measured. To solve this problem, an estimated synchronously rotating $\gamma\delta$ reference frame instead of the actual synchronously rotating dq reference frame is used, as shown in Fig. 1. Then, a position estimation error $\Delta\theta_{re}$ is defined as

$$\Delta\theta_{re} = \hat{\theta}_{re} - \theta_{re} \quad (3)$$

where $\hat{\theta}_{re}$ is the rotor position estimated in the $\gamma\delta$ reference frame.

By transforming (1) into the $\gamma\delta$ reference frame, the back EMF based PMSM model can be expressed as

$$\begin{bmatrix} v_{s\gamma} \\ v_{s\delta} \end{bmatrix} = \begin{bmatrix} R_s + pL_d & -\hat{\omega}_{re} \cdot L_q \\ \hat{\omega}_{re} \cdot L_q & R_s + pL_d \end{bmatrix} \begin{bmatrix} i_{s\gamma} \\ i_{s\delta} \end{bmatrix} + \begin{bmatrix} e_{s\gamma} \\ e_{s\delta} \end{bmatrix} \quad (4)$$

where $v_{s\gamma}$ and $v_{s\delta}$ are the γ- and δ-axis stator voltages, respectively; $i_{s\gamma}$ and $i_{s\delta}$ are the γ- and δ-axis stator currents, respectively; $\hat{\omega}_{re}$ is the estimated rotor electrical angular speed; and $e_{s\gamma}$ and $e_{s\delta}$ are the γ- and δ-axis back EMF components, which can be expressed as

$$\begin{bmatrix} e_{s\gamma} \\ e_{s\delta} \end{bmatrix} = \eta \begin{bmatrix} -\sin\Delta\theta_{re} \\ \cos\Delta\theta_{re} \end{bmatrix} + (\hat{\omega}_{re} - \omega_{re}) \cdot L_q \begin{bmatrix} -i_{s\gamma} \\ i_{s\delta} \end{bmatrix}. \quad (5)$$

According to (5), if $\hat{\omega}_{re} \approx \omega_{re}$, $\Delta\theta_{re}$ can be calculated as $\Delta\theta_{re} = -\tan^{-1}(e_{s\gamma} / e_{s\delta})$. Let $f_{e\gamma} = -e_{s\gamma}/L_d$ and $f_{e\delta} = -e_{s\delta}/L_d$ be the γ- and δ-axis unknown external disturbances, respectively, which contain the information of the γ- and δ-axis back EMF components, respectively, and the rotor position estimation error. Then, the current model of the PMSM can be written as

$$\begin{cases} pi_{s\gamma} = v_{s\gamma}/L_d + f_\gamma + f_{e\gamma} \\ pi_{s\delta} = v_{s\delta}/L_d + f_\delta + f_{e\delta} \end{cases} \quad (6)$$
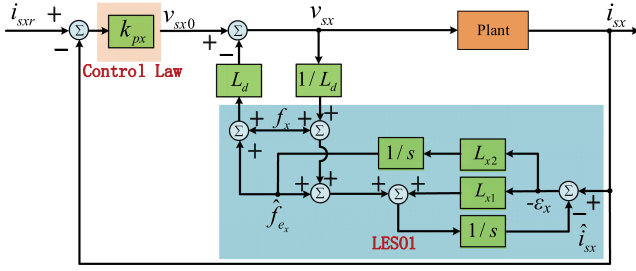
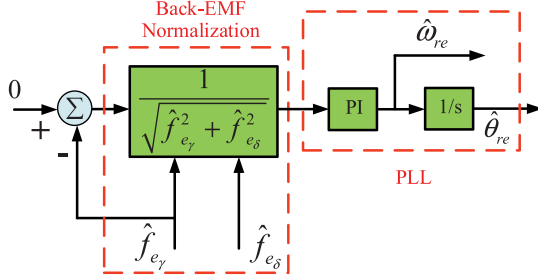Fig. 2.　Block diagram of the plant controlled by the LADRC scheme.

Fig. 3.　Block diagram of the tracking controller for rotor position and speed estimation.

where $f_\gamma = \hat{\omega}_{re} \cdot L_q \cdot i_{s\delta}/L_d - R_s \cdot i_{s\gamma}/L_d$ and $f_\delta = -\hat{\omega}_{re} \cdot L_q \cdot i_{s\gamma}/L_d - R_s \cdot i_{s\delta}/L_d$, which represent the γ- and δ-axis known model information, respectively.

Then, a LESO-based external disturbance observer LESO1 can be designed as follows and is illustrated in Fig. 2:

$$
\begin{cases}
p\hat{i}_{sx} = v_{sx}/L_d + f_x + \hat{f}_{e_x} - L_{x1} \cdot \varepsilon_x \\
p\hat{f}_{e_x} = -L_{x2}\varepsilon_x
\end{cases}, \quad x = \gamma \text{ and } \delta \quad (7)
$$

where $\hat{i}_{sx}$ is the estimated γ/δ-axis stator current; $\varepsilon_x = \hat{i}_{sx} - i_{sx}$ is the γ/δ-axis current estimation error; $\hat{f}_{e_x}$ is the estimated γ/δ-axis unknown external disturbance; and L_{x1} and L_{x2} are the gains of the LESO1. Then, a simple tracking controller [20], [21] can be implemented to estimate the rotor position and speed by simply using a PLL to regulate the normalized value of the estimated γ-axis unknown external disturbance $\hat{f}_{e_\gamma}$, which contains the rotor position error information, to be zero, as shown in Fig. 3. The back EMF normalization guarantees a constant linear dynamic response of the tracking controller regardless of the operating fundamental frequency.

Compared with the conventional SMO-based rotor position estimation, there are two improvements in the proposed scheme. First, by applying the estimated synchronously rotating reference frame instead of the stationary reference frame in the SMO-based method, the back EMF is transformed into the dc components, which removes the need for the low-pass filter in the SMO-based method and, therefore, eliminates the phase delay in the estimated rotor position. Second, due to the use of a continuous integrator $1/s$ in the LESO1 to estimate the back EMF components, the chattering problem caused by the discrete sliding-mode function in the SMO is eliminated.

B. Design of the LADRC-Based Current Controller

According to the ADRC theory [16], the estimated external disturbance can be used as a feedforward compensation term for the input of the plant. Therefore, the final control law of the plant is designed as follows:

$$
v_{sx} = v_{sx0} - L_d \left(f_x + \hat{f}_{e_x} \right) \quad (8)
$$

where v_{sx0} is the plant input generated by the initial control law.

Substituting (8) into (6) yields

$$
p\hat{i}_{sx} = v_{sx0}/L_d - (f_x + \hat{f}_{e_x}) + f_x + f_{e_x} \approx v_{sx0}/L_d. \quad (9)
$$

Then, the plant combined with the LESO1, as shown in Fig. 2, is equivalent to an integrator $1/s$ in the Laplace domain. Then, a simple proportional current controller, as expressed by (10), can be designed to generate the voltage output v_{sx0}, which is compensated by the disturbance estimated by the LESO1, as expressed by (8), to generate the voltage output v_{sx} of the LADRC-based current controller

$$
v_{sx0} = k_{px} \cdot (i_{sxr} - i_{sx}) \quad (10)
$$

where k_{px} is the proportional gain and can be selected as the desired bandwidth of the current loop, which is determined as a tradeoff between the steady-state and transient performance.

III. PROPOSED ELADRC-BASED SENSORLESS FOC SCHEME CONSIDERING PMSM PARAMETER VARIATIONS

A. ELADRC-Based Rotor Position Estimation Algorithm

Since the LESO1 is designed based on the current model, the current regulation quality will also affect the accuracy of the position estimation. According to (7), machine parameters are still needed in the design of the LESO-based sensorless FOC scheme; and the variations of the machine parameters in the LESO1 will affect the current regulation quality, especially when both the d- and q-axis inductances have cross saturations.

The current model of the salient-pole PMSM considering the parameter variations is expressed as

$$
\begin{cases}
p i_{s\gamma} = v_{s\gamma}/L_{d0} + f_\gamma + \hat{f}_{e_\gamma} + f_{id_\gamma} \\
p i_{s\delta} = v_{s\delta}/L_{d0} + f_\delta + \hat{f}_{e_\delta} + f_{id_\delta}
\end{cases} \quad (11)
$$

where f_{id_γ} and f_{id_δ} represent the γ- and δ-axis unknown internal disturbances and are defined as follows:

$$
f_{id_\gamma} = -\frac{\Delta R_s}{L_{d0}} \cdot i_{s\gamma} - p\frac{\Delta L_d}{L_{d0}} \cdot i_{s\gamma} + \frac{\hat{\omega}_{re}}{L_{d0}}\Delta L_q \cdot i_{s\delta}
$$

$$
- \left[\frac{(\Delta L_d - \Delta L_q)}{L_{d0}}(-p \cdot i_{s\delta} + \hat{\omega}_{re} \cdot i_{s\gamma}) + \frac{\hat{\omega}_{re} \cdot \Delta \psi_m}{L_{d0}} \right]
$$

$$
(-\sin\Delta\theta_{re})
$$

$$
f_{id_\delta} = -\frac{\Delta R_s}{L_{d0}} \cdot i_{s\delta} - p\frac{\Delta L_d}{L_{d0}} \cdot i_{s\delta} - \frac{\hat{\omega}_{re}}{L_{d0}}\Delta L_q \cdot i_{s\gamma}
$$

$$
- \left[\frac{(\Delta L_d - \Delta L_q)}{L_{d0}}(-p \cdot i_{s\delta} + \hat{\omega}_{re} \cdot i_{s\gamma}) + \frac{\hat{\omega}_{re} \cdot \Delta \psi_m}{L_{d0}} \right]
$$

$$
(\cos\Delta\theta_{re})
$$

Fig. 4. Block diagram of the plant controlled by the ELADRC scheme.

Fig. 5. Block diagram of the ELADRC-based sensorless FOC scheme for a PMSM drive.

where $\Delta R_s = R_s - R_{s0}$; $\Delta L_d = L_d - L_{d0}$; $\Delta L_q = L_q - L_{q0}$; $\Delta \psi_m = \psi_m - \psi_{m0}$; R_s, L_d, L_q, and ψ_m are the actual parameter values; and R_{s0}, L_{d0}, L_{q0}, and ψ_{m0} denote the nominal parameter values. Thus, the internal disturbances f_{id_γ} and f_{id_δ} contain the information of parameter variations as well as the steady-state (e.g., $i_{s\gamma}$ and $i_{s\delta}$) and transient (e.g., $pi_{s\delta}$) current regulation quality.

Then, another LESO cascaded with the LESO1, called LESO2, is designed as follows to estimate the γ- and δ-axis unknown internal disturbances:

$$\begin{cases} p\hat{i}_{smx} = v_{sx}/L_{d0} + f_x + \hat{f}_{e_x} + \hat{f}_{id_x} - L_{x3}\varepsilon_{mx} \\ p\hat{f}_{id_x} = -L_{x4}\varepsilon_{mx} \end{cases}, \quad x = \gamma \text{ and } \delta \tag{12}$$

where $\hat{i}_{smx}$ is the estimated γ/δ-axis stator current component; $\varepsilon_{mx} = \hat{i}_{smx} - i_{sx}$ is the γ/δ-axis current estimation error; $\hat{f}_{id_x}$ represents the estimated γ/δ-axis unknown internal disturbance; and L_{x3} and L_{x4} are the gains of the LESO2.

B. Design of the ELADRC-Based Current Controller

The estimated internal disturbance is added to the external disturbance to form the total disturbance, which is then used as a feedforward compensation term for the input of the plant. The final control law of the plant is designed as follows:

$$v_{sx} = v_{sx0} - L_{d0}\left(f_x + \hat{f}_{e_x} + \hat{f}_{id_x}\right). \tag{13}$$

Substituting (13) into (11) yields

$$pi_{sx} = v_{sx0}/L_{d0} - \left(f_x + \hat{f}_{e_x} + \hat{f}_{id_x}\right) + f_x + \hat{f}_{e_x} + \hat{f}_{id_x}$$
$$\approx v_{sx0}/L_{d0}. \tag{14}$$

The plant combined with the two LESOs, as shown in Fig. 4, is equivalent to an integrator $1/s$. Then, the proportional current controller, as expressed by (10), is used to generate the voltage output v_{sx0}, which is compensated by the estimated total disturbance, as expressed by (13), to generate the voltage output v_{sx} of the ELADRC-based current controller to control the plant. By compensating the plant input with the estimated unknown internal disturbance $\hat{f}_{id_x}$, both the steady-state and transient current regulation quality of the ELADRC scheme are improved compared to that of the LADRC scheme, which further improves the rotor position estimation accuracy. Fig. 5 shows the block diagram of the overall ELADRC-based position sensorless FOC scheme for a PMSM drive, where the PMSM, inverter, space-vector pulsewidth modulation (SVPWM), and coordinate transformation blocks form the plant in Figs. 3 and 4.

IV. PARAMETER DESIGN AND PERFORMANCE ANALYSIS FOR THE ELADRC

A. Stability Analysis and Parameter Design for the ELADRC

First of all, the stability of the LESO1 is investigated. Let $e = [\hat{i}_{sx} - i_{sx}, \ \hat{f}_{e_x} - f_{e_x}]^T$ be the tracking error of the LESO1. According to (6) and (7), the error state equation can be derived as

$$\dot{e} = A_m e \tag{15}$$

where $A_m = \begin{bmatrix} -L_{x1} & 1 \\ -L_{x2} & 0 \end{bmatrix}$. Equation (15) shows that the eigenvalues of A_m determine the behavior of the LESO1. If and only if $L_{x2} > 0$, the error dynamics (15) is asymptotically stable.

The parameters of the LESO1 can simply be designed according to the desired bandwidth of the LESO1 [22]. Specifically, in this work, the parameters of the LESO1 are designed such that the matrix A_m has a double eigenvalue λ that is equal to the bandwidth of the LESO1. Thus, the following equation should be satisfied:

$$|\lambda E - A_m| = \begin{vmatrix} \lambda + L_{x1} & -1 \\ L_{x2} & \lambda \end{vmatrix}$$
$$= \lambda^2 + L_{x1}\lambda + L_{x2} = (\lambda + \omega_0)^2 \tag{16}$$

where ω_0 is viewed as the bandwidth of the LESO1, which should be large enough to ensure that the dynamic of the LESO1 is sufficiently fast to track the variation of the disturbance. Once ω_0 is chosen, the LESO1 parameters can be determined, according to (16), to be $L_{x1} = 2\omega_0$ and $L_{x2} = \omega_0^2$.

The stability analysis and parameter design for the LESO2 are the same as those for the LESO1. The current controller parameter k_p is usually chosen to be 1/5–1/3 of ω_0 [22].

B. Tracking Performance Analysis for the ELADRC

A timely and accurate estimation of the external disturbance is essential to ensure the tracking performance of the ELADRC. According to (6) and (7), the relationship between the estimated value $\hat{f}_{e_x}$ and the actual value f_{e_x} of the external disturbance in the frequency domain can be deduced as follows:

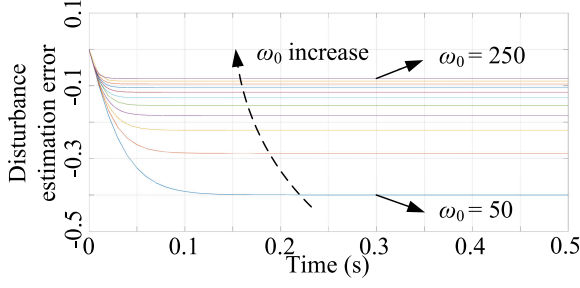$$\frac{\hat{F}_{e_x}(s)}{F_{e_x}(s)} = \frac{L_{x2}}{s^2 + L_{x1}s + L_{x2}}. \tag{17}$$

Fig. 6. Time-domain response of external disturbance estimation error at different bandwidths.
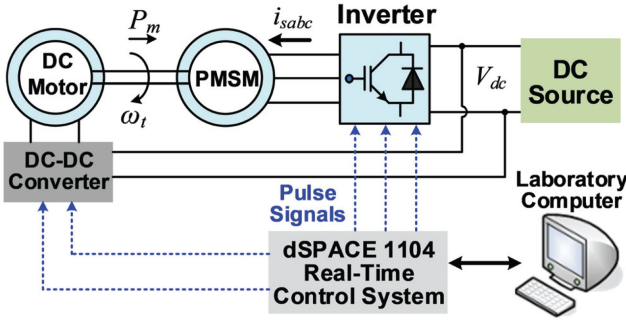
Fig. 7. Block diagram of the experimental system.
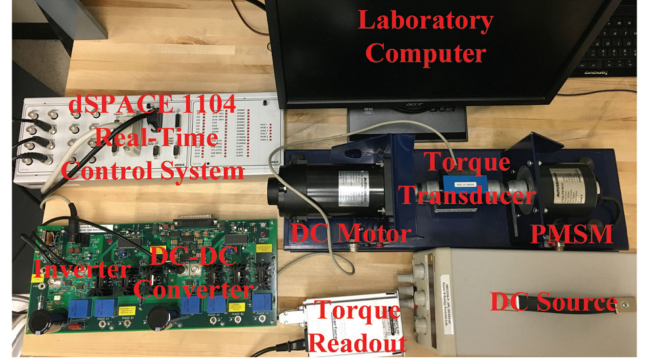

Fig. 8. Hardware setup of the experimental system.

TABLE I
PARAMETERS OF THE PMSM AND EXPERIMENTAL SYSTEM

	Parameter	Value	Parameter	Value
	Rated Speed	1500 rpm	Stator Resistance	0.268 Ω
	Rated Power	275 W	d-axis Inductance	1.12 mH
PMSM	Rated Load Torque	1.8 N·m	q-axis Inductance	1.51 mH
	Moment of Inertia	7e-6 kg·m²	Flux Linkage	0.0191 V·s
	Voltage Constant	13.5 V/rpm	# of Pole Pairs	2
Inverter	DC-Bus Voltage	41.75 V	Switching Frequency	10 kHz
Control System	Dead time	1 μs	Sampling Period	100 μs
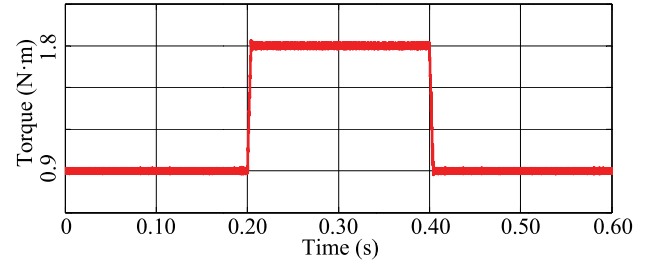
Fig. 9. Load torque for evaluating the four sensorless FOC schemes.

Then, the transfer function between the external disturbance estimation error and the actual external disturbance is

$$\frac{\hat{F}_{e_x}(s) - F_{e_x}(s)}{F_{e_x}(s)} = -\frac{s(s+L_{x1})}{s^2+L_{x1}s+L_{x2}} = -\frac{s(s+2\omega_0)}{s^2+2\omega_0 s+\omega_0^2}. \tag{18}$$

Under a ramp-change excitation, i.e., the actual external disturbance, with a slope of 75, the time-domain response of the external disturbance estimation error is obtained, according to (18), and plotted in Fig. 6 for different bandwidths ω_0 changing from 50 to 250 rad/s with an increment of 20 rad/s. The results show that the bandwidth of the LESO1 has a significant impact on the disturbance estimation accuracy. When the bandwidth is higher, the disturbance estimation error becomes smaller and the tracking speed becomes faster. The tracking performance of the LESO2 can be analyzed in the same way.

V. EXPERIMENTAL RESULTS

A. Experimental Setup

Experimental studies are carried out for a 275-W salient-pole PMSM drive to evaluate the proposed ELADRC-based rotor position sensorless FOC scheme in comparison with the conventional [24] and adaptive [4] SMO-based sensorless FOC schemes and the LADRC-based sensorless FOC scheme. The PMSM is similar to the traction motor used in Toyota Prius but has a reduced scale. The block diagram and the hardware setup of the experimental system are shown in Figs. 7 and 8, respectively. The parameters of the PMSM and experimental system are listed in Table I. The FOC schemes are implemented in a dSPACE 1104 real-time control system. The same PI controller with

a bandwidth of 28.5 Hz is used for the speed loops of the four different sensorless FOC schemes. In the conventional and adaptive SMO-based sensorless FOC schemes, the bandwidth of the PI controllers used in the current loop is chosen to be 2000 Hz according to Astrom and Hagglund [23]. Moreover, the parameters of the LADRC- and ELADRC-based sensorless FOC schemes are the same: the bandwidth of the LESO1 and LESO2 is chosen to be 2000 Hz as a tradeoff between the current tracking performance and immunity to noise, and the proportional gain K_p of the current controller is set as 500.

B. Sudden Load Torque Changes at a Constant Speed Without PMSM Parameter Mismatch

The rotor position and speed estimation performance of the four sensorless FOC schemes is compared for the salient-pole PMSM operating at 1500 r/min, where the load torque is changed from 0.9 to 1.8 N·m and then back to 0.9 N·m with a slope of 75 N·m/s, as shown in Fig. 9. The corresponding rotor positions,
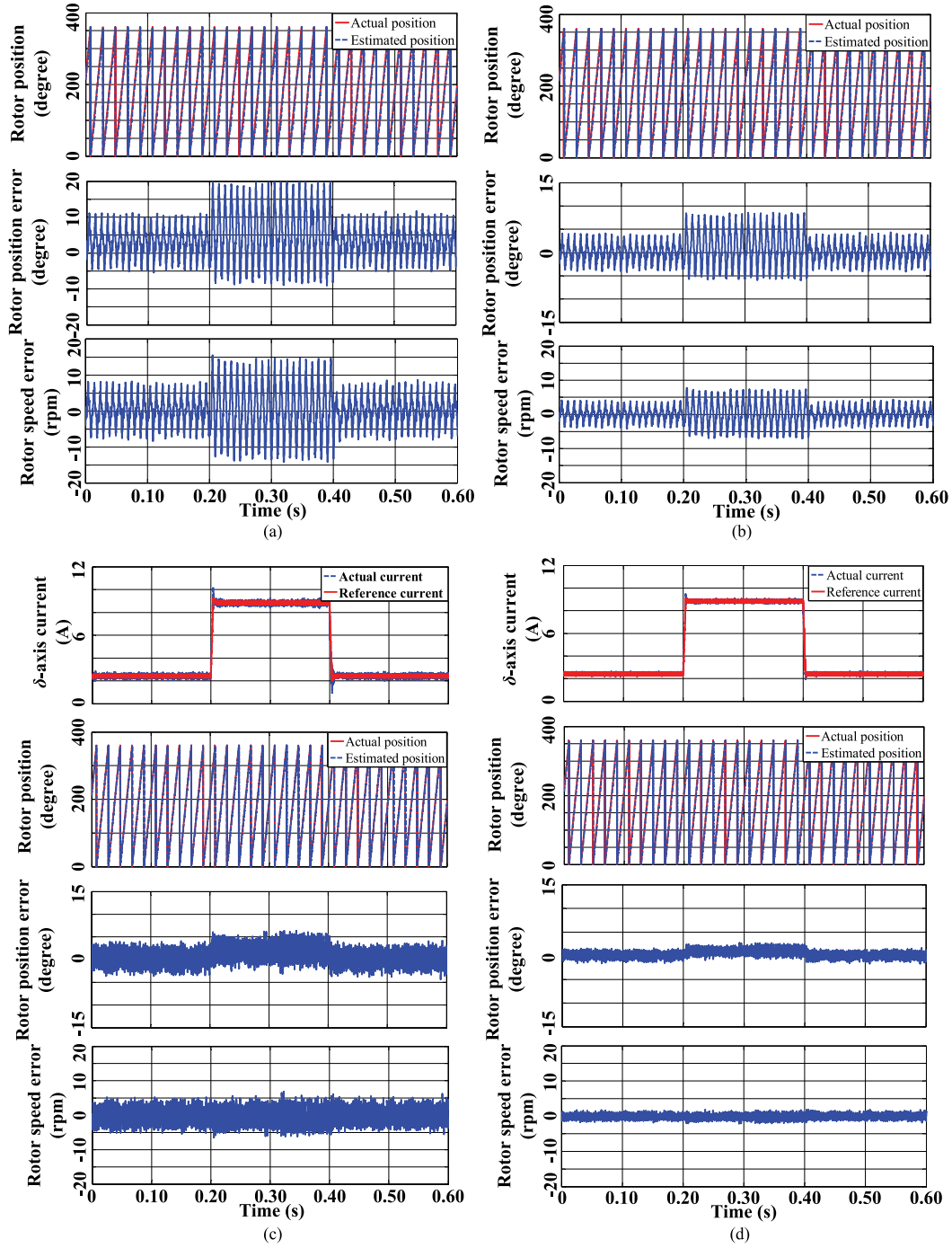
Fig. 10. Test results under sudden load torque changes: (a) conventional SMO-, (b) adaptive SMO-, (c) LADRC-, and (d) ELADRC-based sensorless FOC schemes.

TABLE II
PERFORMANCE COMPARISON OF THE FOUR SENSORLESS FOC SCHEMES UNDER CONSTANT SPEED WITH SUDDEN LOAD TORQUE CHANGES

Performance Metric	Before/After Sudden Load Torque Change			
	Conventional SMO	Adaptive SMO	LADRC	ELADRC
Amplitude of rotor position estimation error (degree)	8.2/16	4.5/8	4/6	2.5/3
Amplitude of rotor speed estimation error (rpm)	8/15.3	4.9/7	4.7/5.2	1/1.2
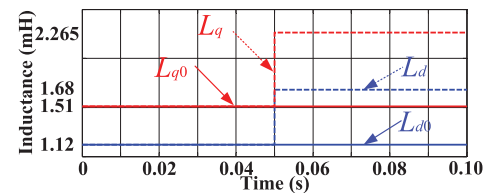
Fig. 11. Mismatch of the d- and q-axis inductances used by the four sensorless FOC schemes.
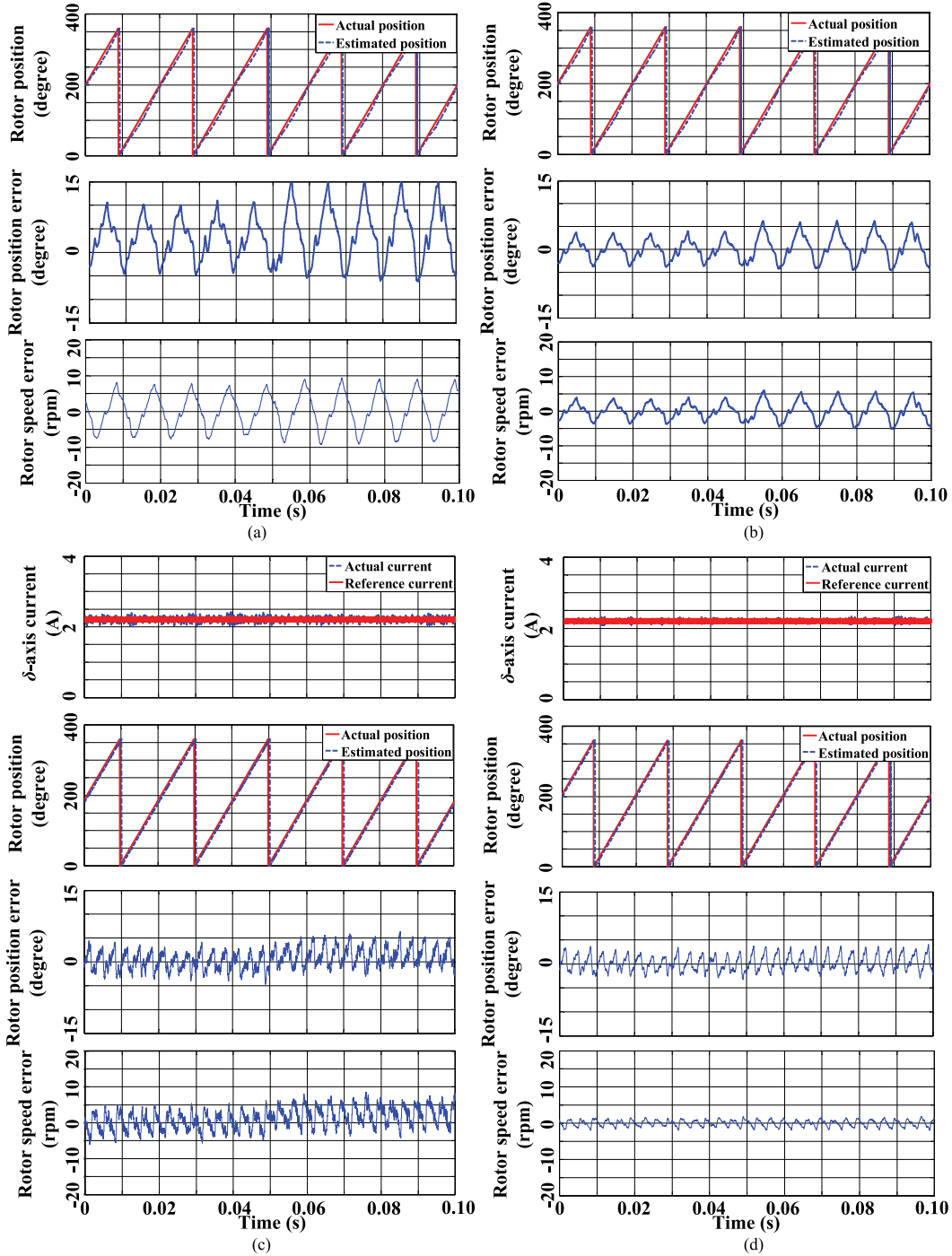
Fig. 12.   Test results with an inductance mismatch: (a) conventional SMO-, (b) adaptive SMO-, (c) LADRC-, and (d) ELADRC-based sensorless FOC schemes.

rotor position estimation errors, and the rotor speed estimation errors of the system using the four sensorless FOC schemes are compared in Fig. 10 and Table II. These results show that before the load torque changes, the proposed ELADRC-based sensorless FOC scheme has the smallest position and speed estimation errors among the four sensorless FOC schemes, and the proposed LADRC-based sensorless FOC scheme is also better than the two SMO-based schemes. Compared to the conventional SMO-based scheme, the rotor position waveforms of the adaptive SMO-based scheme have no dc offset, which means that there is no phase delay problem. However, there is still the chattering problem. For the proposed LADRC-based and ELADRC-based schemes, both the phase delay and the chatting problem presented in the SMO-based schemes are significantly mitigated. As discussed at the end of Section II-A, these improvements are due to the estimation of the back EMF in the estimated synchronously rotating reference frame instead of the stationary reference frame in the SMO-based schemes and
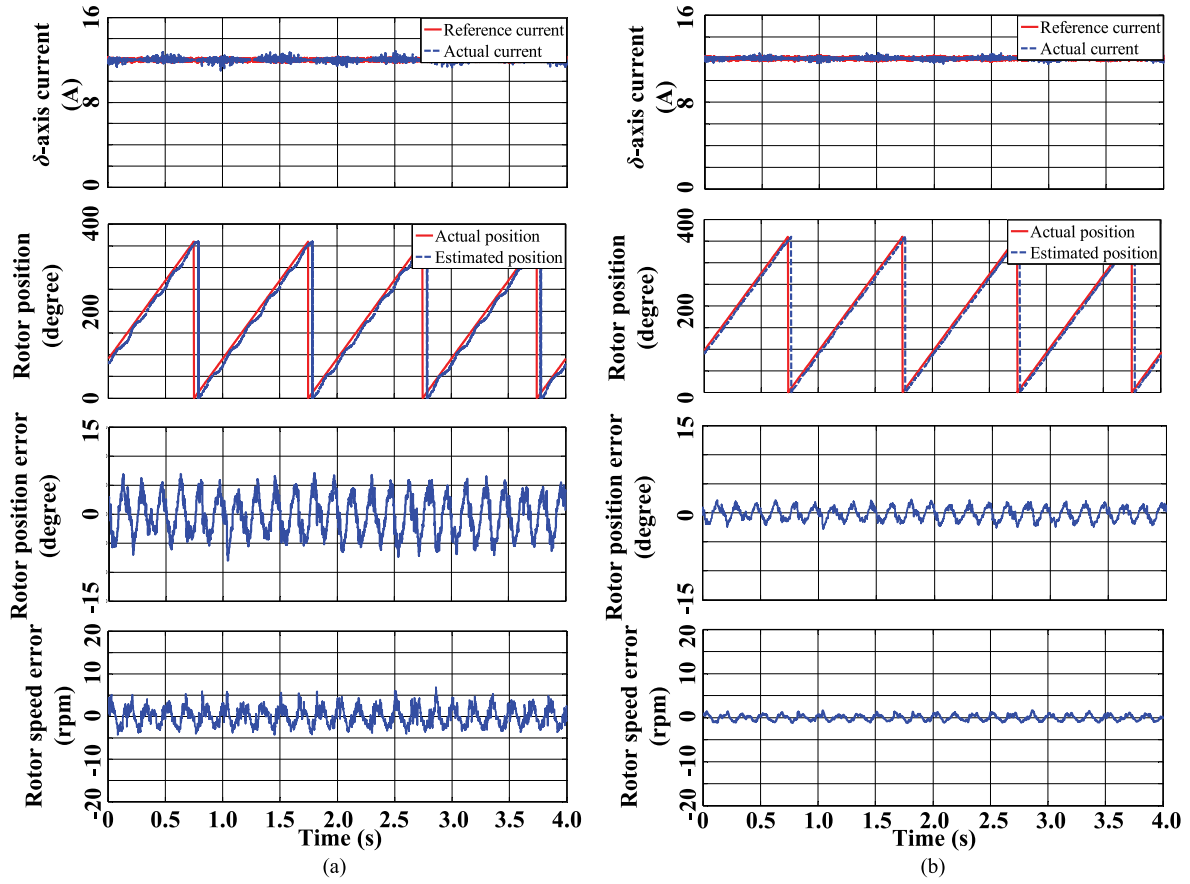
Fig. 13.   Test results under a low speed with a large load torque: (a) LADRC- and (b) ELADRC-based sensorless FOC schemes.

the use of a continuous integrator $1/s$ in the LESO1 to estimate the back EMF components. The former ensures no phase delay problem while the latter significantly mitigates the chattering problem.

When the load torque changes suddenly, the rotor position and the speed estimation errors only increase slightly when using the ELADRC-based scheme but increase more significantly when using the other three schemes, particularly the two SMO-based schemes. With the help of the LESO2 to estimate and compensate for the internal disturbance, the current regulation quality of the ELADRC-based scheme is better than that of the LADRC-based scheme in both the steady-state and transient conditions, as shown in the PMSM δ-axis current plots in Fig. 10(c) and (d). Thus, the rotor position and speed estimation performance of the ELADRC-based scheme is better than that of the LADRC-based scheme.

C. Constant Load Torque and Constant Speed With PMSM Parameter Mismatch

The rotor position and speed estimation performance of the four sensorless FOC schemes is compared for the salient-pole PMSM operating at 1500 r/min, where the load torque reference is 0.9 N·m. Assume that the d- and q-axis inductances used by the four schemes are mismeasured to be 150% of L_{d0} and L_{q0} from 0.05 s onward, as shown in Fig. 11.

TABLE III
PERFORMANCE COMPARISON OF THE FOUR ROTOR POSITION SENSORLESS
FOC SCHEMES UNDER PARAMETER MISMATCHES

Performance Metric	Before/After Parameter Mismatches			
	Conventional SMO	Adaptive SMO	LADRC	ELADRC
Amplitude of rotor position estimation error (degree)	8.2/12	4.5/5.2	4/4.4	2.5/2.5
Amplitude of rotor speed estimation error (rpm)	8/10	4.9/5.1	4.7/4.9	1/1

The rotor positions, rotor position estimation errors, and the rotor speed estimation errors of the system using the four sensorless FOC schemes are compared in Fig. 12 and Table III. These results show that the ELADRC-based sensorless FOC scheme has the best rotor position and speed estimation performance among the four schemes. When the parameter mismatch occurs, the rotor position and speed estimation errors do not change at all when using the ELADRC-based scheme but increase significantly or obviously when using the other three schemes. The robustness of the ELADRC to the parameter mismatch is achieved by using the LESO2, which estimates the internal disturbance caused by the parameter mismatch and compensates the estimated disturbance in the current control loop to improve the current regulation quality of the ELADRC-based

scheme over the LADRC-based scheme, as shown in the first plots of Fig. 12(c) and (d).

D. Low-Speed Operation With a Large Load Torque

To verify the superior performance of the ELADRC-based sensorless FOC scheme under low-speed conditions, which are more challenging for the back EMF based rotor position sensorless control methods, the salient-pole PMSM with each of the four sensorless FOC schemes was tested at 30 r/min with a load torque of 2.16 N·m, which is 120% of the rated value. At such a low speed and large load torque condition, the two SMO-based sensorless FOC schemes failed to control the PMSM; however, both the LADRC- and the ELADRC-based sensorless FOC schemes controlled the PMSM well, as shown in Fig. 13. With the help of the LESO2 to estimate and compensate for the internal disturbance, the current (e.g., δ-axis current) regulation quality of the ELADRC-based scheme is better than that of the LADRC-based scheme; and the amplitudes of the rotor position and speed estimation errors of the ELADRC-based scheme are 2.5° and 1.1 r/min, respectively, which are much smaller than 6.8° and 5.2 r/min, respectively, of the LADRC-based scheme.

VI. CONCLUSION

An ELADRC-based rotor position sensorless FOC scheme was proposed for the PMSM drives in an estimated synchronously rotating reference frame. The proposed scheme does not have the phase delay or chattering problem as seen in the conventional SMO-based sensorless FOC schemes. In addition, the current regulation quality of the proposed scheme was improved by timely estimating and compensating for the internal disturbances, such as the parameter and current regulation quality variations in the current control loop, which further improved the position estimation performance. The stability of the closed-loop PMSM drive system with the ELADRC-based sensorless FOC scheme was analyzed. Based on the analysis, the parameters of the ELADRC were designed. The performance of the ELADRC-based scheme was validated by the experimental results for a 275-W salient-pole PMSM drive. The experimental results showed that the PMSM drive using the ELADRC-based scheme was not affected by PMSM parameter mismatches at all and had a better rotor position estimation performance than that using the conventional and adaptive SMO-based and the LADRC-based sensorless FOC schemes.

REFERENCES

[1] Y. Zhao, C. Wei, Z. Zhang, and W. Qiao, "A review on position/speed sensorless control for permanent-magnet synchronous machine-based wind energy conversion systems," *IEEE J. Emerg. Sel. Topics Power Electron.*, vol. 1, no. 4, pp. 203–216, Dec. 2013.

[2] G. Wang *et al.*, "Self-commissioning of permanent magnet synchronous machine drives at standstill considering inverter nonlinearities," *IEEE Trans. Power Electron.*, vol. 29, no. 12, pp. 6615–6627, Dec. 2014.

[3] M. Pacas, "Sensorless drives in industrial applications," *IEEE Ind. Electron. Mag.*, vol. 5, no. 2, pp. 16–23, Jun. 2011.

[4] D. Liang, J. Li, R. Qu, and W. Kong, "Adaptive second-order sliding-mode observer for PMSM sensorless control considering VSI nonlinearity," *IEEE Trans. Power Electron.*, vol. 33, no. 10, pp. 8994–9004, Oct. 2018.

[5] W. Xu, Y. Jiang, C. Mu, and F. Blaabjerg, "Improved nonlinear flux observer-based second-order SOIFO for PMSM sensorless control," *IEEE Trans. Power Electron.*, vol. 34, no. 1, pp. 565–579, Jan. 2019.

[6] J. Kim, I. Jeong, K. Nam, J. Yang, and T. Hwang, "Sensorless control of PMSM in a high-speed region considering iron loss," *IEEE Trans. Ind. Electron.*, vol. 62, no. 10, pp. 6151–6159, Oct. 2015.

[7] J. Liu, T. A. Nondahl, P. B. Schmidt, S. Royak, and M. Harbaugh, "Rotor position estimation for synchronous machines based on equivalent EMF," *IEEE Trans. Ind. Appl.*, vol. 47, no. 3, pp. 1310–1318, May/Jun. 2011.

[8] G. H. B. Foo and M. F. Rahman, "Direct torque control of an IPM synchronous motor drive at very low speed using a sliding-mode stator flux observer," *IEEE Trans. Power Electron.*, vol. 25, no. 4, pp. 933–942, Apr. 2010.

[9] X. Luo, Q. Tang, A. Shen, and Q. Zhang, "PMSM sensorless control by injecting HF pulsating carrier signal into estimated fixed-frequency rotating reference frame," *IEEE Trans. Ind. Electron.*, vol. 63, no. 4, pp. 2294–2303, Apr. 2016.

[10] G. Xie, K. Lu, S. K. Dwivedi, J. R. Rosholm, and F. Blaabjerg, "Minimum-voltage vector injection method for sensorless control of PMSM for low-speed operations," *IEEE Trans. Power Electron.*, vol. 31, no. 2, pp. 1785–1794, Feb. 2016.

[11] M. J. Corley and R. D. Lorenz, "Rotor position and velocity estimation for a salient-pole permanent magnet synchronous machine at standstill and high speeds," *IEEE Trans. Ind. Appl.*, vol. 34, no. 4, pp. 784–789, Jul./Aug. 1998.

[12] H. Kim, J. Son, and J. Lee, "A high-speed sliding-mode observer for the sensorless speed control of a PMSM," *IEEE Trans. Ind. Electron.*, vol. 58, no. 9, pp. 4069–4077, Sep. 2011.

[13] Z. Qiao, T. Shi, Y. Wang, Y. Yan, C. Xia, and X. He, "New sliding-mode observer for position sensorless control of permanent-magnet synchronous motor," *IEEE Trans. Ind. Electron.*, vol. 60, no. 2, pp. 710–719, Feb. 2013.

[14] Z. Chen, M. Tomita, S. Doki, and S. Okuma, "An extended electromotive force model for sensorless control of interior permanent magnet synchronous motors," *IEEE Trans. Ind. Electron.*, vol. 50, no. 2, pp. 288–295, Apr. 2003.

[15] S. Morimoto, K. Kawamoto, M. Sanada, and Y. Takeda, "Sensorless control strategy for salient-pole PMSM based on extended EMF in rotating reference frame," *IEEE Trans. Ind. Appl.*, vol. 38, no. 4, pp. 1054–1061, Jul./Aug. 2002.

[16] J. Han, "From PID to active disturbance rejection control," *IEEE Trans. Ind. Electron.*, vol. 56, no. 3, pp. 900–906, Mar. 2009.

[17] B. Sun and Z. Gao, "A DSP-based active disturbance rejection control design for a 1-kW H-bridge dc–dc power converter," *IEEE Trans. Ind. Electron.*, vol. 52, no. 5, pp. 1271–1277, Oct. 2005.

[18] J. Li, H.-P. Ren, and Y.-R. Zhong, "Robust speed control of induction motor drives using first-order auto-disturbance rejection controllers," *IEEE Trans. Ind. Appl.*, vol. 51, no. 1, pp. 712–720, Jan./Feb. 2015.

[19] B. Du, S. Wu, S. Han, and S. Cui, "Application of linear active disturbance rejection controller for sensorless control of internal permanent-magnet synchronous motor," *IEEE Trans. Ind. Electron.*, vol. 63, no. 5, pp. 3019–3027, May 2016.

[20] G. Zhang, G. Wang, D. Xu, R. Ni, and C. Jia, "Multiple-AVF cross-feedback-network-based position error harmonic fluctuation elimination for sensorless IPMSM drives," *IEEE Trans. Ind. Electron.*, vol. 63, no. 2, pp. 821–831, Feb. 2016.

[21] G. Zhang, G. Wang, D. Xu, and Y. Yu, "Discrete-time low-frequency-ratio synchronous-frame full-order observer for position sensorless IPMSM drives," *IEEE J. Emerg. Sel. Topics Power Electron.*, vol. 5, no. 2, pp. 870–879, Jun. 2017.

[22] Z. Gao, "Scaling and bandwidth-parameterization based controller tuning," in *Proc. Amer. Control Conf.*, Jun. 2003, pp. 4989–4996.

[23] K. J. Astrom and T. Hagglund, *Advanced PID Control*. Research Triangle, NC, USA: Instrumentation, Syst., Automation Society, 2006.

[24] Y. Zhao, W. Qiao, and L. Wu, "Improved rotor position and speed estimators for sensorless control of interior permanent-magnet synchronous machines," *IEEE J. Emerg. Sel. Topics Power Electron.*, vol. 2, no. 3, pp. 627–639, Sep. 2014.

Lizhi Qu (S'19) received the B.Eng. and M.Eng. degrees in electrical engineering from the Harbin Institute of Technology, Harbin, China, in 2013 and 2015, respectively. He is currently working toward the Ph.D. degree in electrical engineering with the University of Nebraska–Lincoln, Lincoln, NE, USA.

He was an Electrical Engineering Intern with Ford Motor Company in summer 2018. His current research interests include power electronics and electric motor drives.

Liyan Qu (S'05–M'08–SM'17) received the B.Eng. (with the highest distinction) and M.Eng. degrees from Zhejiang University, Hangzhou, China, in 1999 and 2002, respectively, and the Ph.D. degree from the University of Illinois at Urbana–Champaign, Champaign, IL, USA, in 2007, all in electrical engineering.

From 2007 to 2009, she was an Application Engineer with Ansoft Corporation, Irvine, CA, USA. Since January 2010, she has been with the University of Nebraska−Lincoln, Lincoln, NE, USA, where she is currently an Associate Professor with the Department of Electrical and Computer Engineering. Her research interests include energy efficiency, renewable energy, numerical analysis and computer-aided design of electric machinery and power electronic devices, dynamics and control of electric machinery, and magnetic devices.

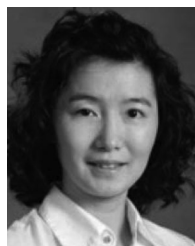Dr. Qu was the recipient of a 2016 U.S. National Science Foundation CAREER Award.

Wei Qiao (S'05–M'08–SM'12) received the B.Eng. and M.Eng. degrees in electrical engineering from Zhejiang University, Hangzhou, China, in 1997 and 2002, respectively, the M.S. degree in high-performance computation for engineered systems from Singapore–MIT Alliance, Singapore, in 2003, and the Ph.D. degree in electrical engineering from the Georgia Institute of Technology, Atlanta, GA, USA, in 2008.

Since August 2008, he has been with the University of Nebraska–Lincoln, Lincoln, NE, USA, where he is currently a Professor with the Department of Electrical and Computer Engineering. His research interests include renewable energy systems, smart grids, condition monitoring, power electronics, electric motor drives, energy storage systems, and emerging electrical energy conversion devices. He is the author or coauthor of more than 240 papers in refereed journals and conference proceedings and holds eight U.S. patents issued.

Dr. Qiao is an Editor for the IEEE TRANSACTIONS ON ENERGY CONVERSION and an Associate Editor for the IEEE TRANSACTIONS ON POWER ELECTRONICS and the IEEE JOURNAL OF EMERGING AND SELECTED TOPICS IN POWER ELECTRONICS. He was the recipient of a 2010 U.S. National Science Foundation CAREER Award and the 2010 IEEE Industry Applications Society Andrew W. Smith Outstanding Young Member Award.